공학석사학위논문

전기분사 공정을 이용한 고체산화물 연료전지 제작에서 증착온도가 미치는 영향

Effect of Deposition Temperature during Electrospray Fabrication of Solid Oxide Fuel Cells

2017년 8월

서울대학교 대학원

기계항공공학부

Guangmin Li

Abstract

Guangmin Li

Department of Mechanical and Aerospace Engineering

The Graduate School

Seoul National University

Ceramics can play a remarkable role in the engineering of intermediate temperature solid oxide fuel cells(IT-SOFCs) capable of meeting the ambitious targets of reduced cost and improved lifetime. The electro-spray deposition(ESD) method has been successfully applied to fabricate the dense Yttria-stabilized Zirconia(YSZ) electrolyte layer and Gadolinium-doped Ceria(GDC) buffer layer of the Solid Oxide Fuel Cells with ceramic powders. In our experiment, we applied ESD method to fabricate the uniform and porous GDC-Lanthanum strontium cobaltite(LSC) cathode functional layer(CFL) and LSC current collector cathode layer(CCCL). The ESD process is proceeded with the electro-spray precursor solution which is composed with different ceramic powders and polyvinyl-pyrrolidone(PVP) or polyvinyl butyral(PVB) additives. In this thesis, we mainly explore the change of the structure and morphology of cathode with the different deposition temperature via electro-spray process and by utilizing the results of scanning electron microscopy(SEM) images and advanced rheometric expansion system(ARES), we analyze the reasons and put forward to some credible assumptions which can account for the results. Ultimately, by comparing the electrochemical characterization of the SOFCs, we extrude the superiority of the crack-free cells and conclude a simple and convenient way to fabricate crack-free and uniform cathode layers in PVP-assisted SOFCs.

Keywords: Solid Oxide Fuel Cells, polyvinyl –pyrrolidone, cracks, electrospray, deposition temperature

Student Number: 2015-22304

Contents

List of Figures

List of Tables

Chapter 1. Introduction

Thin film solid oxide fuel cells(SOFCs) have attracted world-wide research interest because of their huge potential for power generation in stationary and potentially high energy-density. They also have advantages like the pretty lower emissions of sulfur and nitrogen oxides, significant reduction of CO_2 emissions and the convenience of directly converting chemical energy into electrical energy.

There are several ways to fabricate the SOFCs, like screen printing, atomic layer deposition(ALD) and pulsed laser deposition(PLD). Among them, the screen printing technique is the most widely used process because of its convenience and character of quantity production. However, during the screen printing process, it is hard to fabricate the precursor and difficult to apply surface patterning. ALD and PLD process may have potential to fabricate the SOFCs with higher performance because of their thinner layer deposition technique but both of the process need more rigorous condition like vacuum circumstance, and they are both difficult for quantity production.

In this paper, we employed the electro-spray method to fabricate the SOFCs. Electro-spray deposition is the technique using the nozzle filling with the specific precursor solution and in the condition of high voltage, the solution would emit from the metal tip in the shape of nano-scaled liquid drop. The liquid drop would be uniformly deposited on the sample which was displayed on the grounded metal plate. The spray precursor solution was consisting of ethanol

solvent, ceramic powder as well as polymer(PVP or PVB) dispersant. The whole process was easily controlled by adjusting the voltage or changing the content of spray precursor.

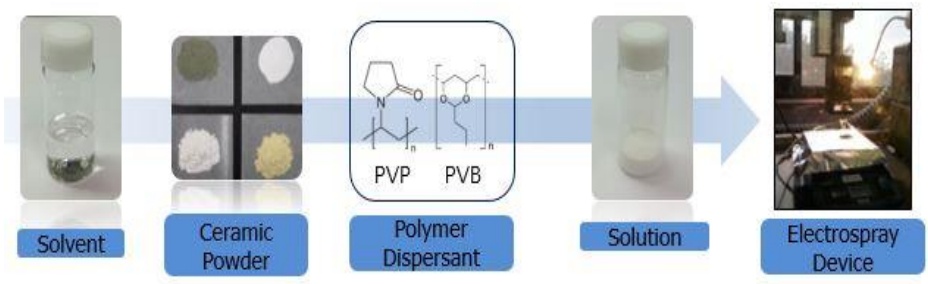

Figure 1 Preparation process of the EDS precursor solution

The electro-spray deposition technique provides the potential to produce a large variety of ceramic thin films. And comparing with other deposition techniques, the ESD technique is particularly advantageous in changing the film morphology by adjusting the deposition conditions, films of different surface morphologies, ranging from dense to very porous, were obtained by ESD. In addition, the ESD process gives the advantages of simple and cheap device, ease of upscaling, wide choice of precursors, high deposition efficiency, easy composition control, and flexible ambient atmosphere operation. In a word, ESD is a fast and convenient way to deposit pure, composite or graded oxide layers. It is less expensive than other deposition techniques, which typically require vacuum process or complicated precursor, and it is also highly flexible, allowing

for a large selection of materials to be deposited.

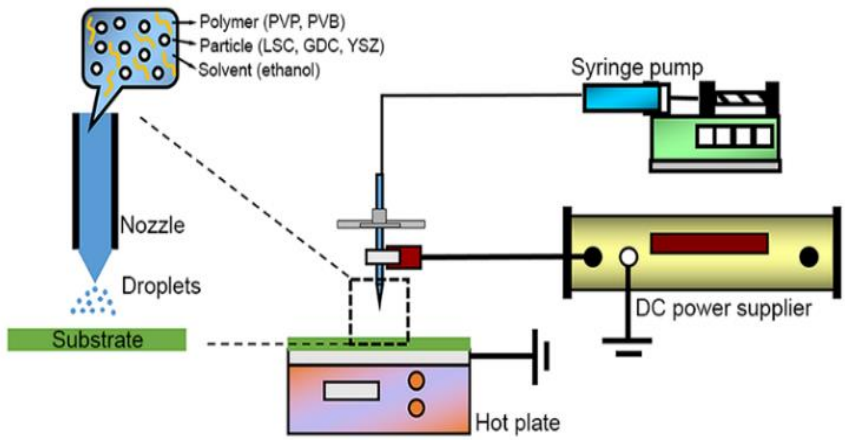

Figure 2 Schematic illustrations of polymer-assisted ESD process

However, during the experiment of fabricating the SOFCs using polymer assisted ESD process, the cathode may arise the problem like de-bonding phenomena or cracks formation. These kinds of phenomena ultimately influence the total performance of SOFCs since they will reduce the reaction area in cathode layers and influence the ion conducting pathway between the electrolyte and cathode. We assumed that the polymer we used in the deposition process may be the main reason that caused these kinds of problems and through the experiments, we concluded that the cathode' structure and morphologies would change a lot with the different deposition temperature via ESD process. In this thesis, we reported a systematic study of the influence of the deposition temperature in the polymer assisted ESD process and put

forward to some credible assumptions to our results.

Chapter 2. SOFCs' fabrication process

During the experiment, we utilized the commercial cell (NaraCellTech) which was composed of NiO-YSZ anode and YSZ electrolyte. The anode was made by powder pressing process with NiO and YSZ granules mixing with polymethylmethacrylate(PMMA). The electrolyte was made by screen printing process and composed of Yttria-stabilized Zirconia(YSZ) whose thickness was around 4~5 μm. GDC buffer layer and composed cathode layer were deposited on it. Disks of commercial cell were about 20 mm in diameter and 1 mm in thickness.

Composite cathodes were composed of cathode functional layer(CFL) and cathode current collector layer(CCCL). CFL is a mixture of LSC and the buffer layer material GDC, it is regarded as promising cathodes for the intermediate temperature solid oxide fuel cells. Also, the CFL will prevent the thermal mismatch during the high temperature annealing process between the cathode and electrolyte. The more porous CCCL is composed of the pure LSC, whose structure can promote the gas diffusion. The composite electrodes not only provide very effective electronic and ionic pathways to electrode/ electrolyte interfaces, but also enhance the injection of mobile charged oxygen surface species into the YSZ electrolyte. In addition, the CFL consisting of the GDC and the LSC have better electrochemical performance than the cathode consisting

of LSC alone.

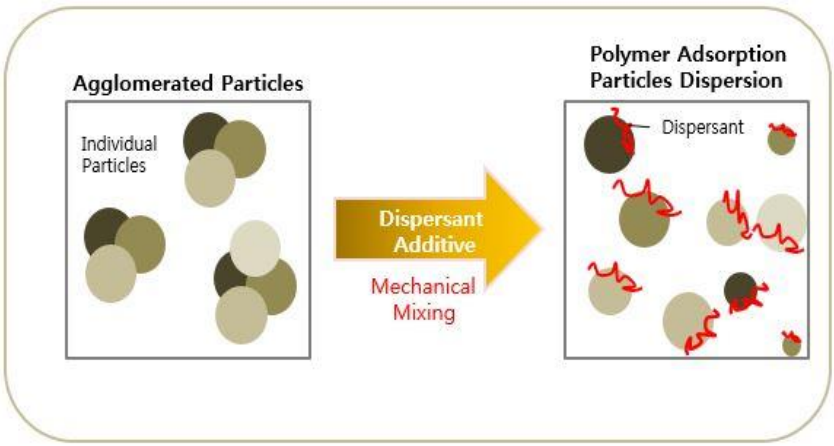

Figure 3 Schematic illustrations of the function of dispersant

During the process of the polymer-assisted electro spray deposition to fabricate a SOFC, the polymer plays the role of dispersant in the precursor solvent. They enhance the powders to be more dispersive. Each dispersant unit adhere to the individual particles' surface and divide the particles from agglomeration. After dispersive, they also prevent the particles from re-agglomeration due to electrostatic repulsion and steric repulsion, meanwhile, control the sedimentation and formation.

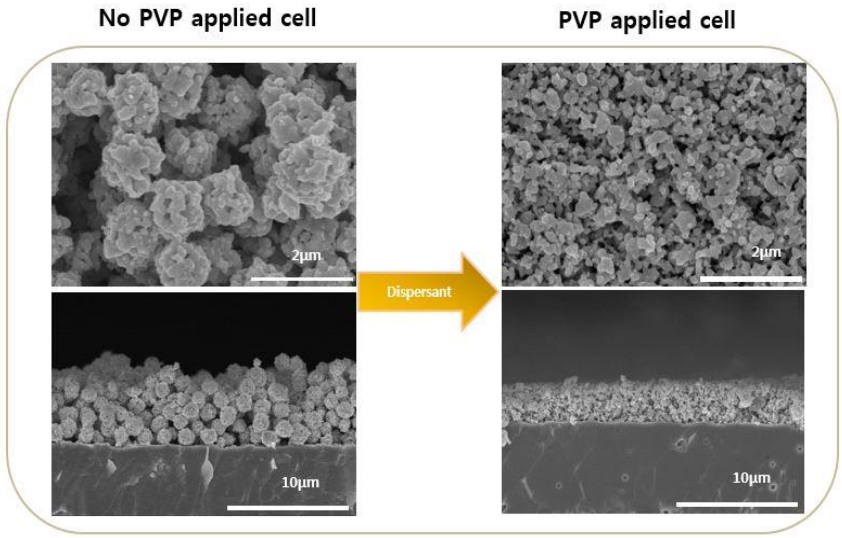

Figure 4 Difference between PVP applied LSC cathode and not applied cathode

Figure 4 shows the difference between the PVP-applied LSC cathode and only LSC ceramic powders deposited cathode. We can definitely find that in the only LSC powder applied cathode, the powders get agglomerated and present the ball-shaped morphology. On the contrary, in the PVP-assisted LSC cathode, the particles are more dispersive and uniform so that increase the reaction area and enhance the final performance of the cells. Therefore, the polymer utilization is very important in the ESD process.

2.1. GDC layer fabrication

Since the chemical reaction between the LSC and the YSZ may cause a degradation to the composite cathode, we need to deposit a thin GDC layer between the YSZ electrolyte and composite cathodes layers to avoid the direct contact. This kind of GDC thin layer is named after buffer layer or barrier layer, however, this layer will participate in the electrochemical process during the cells' working time. Since the GDC layer will increase the ohmic loss, we should deposit the GDC layer as thin as possible to insure the final performance of the cells.

The precursor solution of the GDC layer is consisting of GDC powder (Rhodia, 640nm) and PVB dispersant(Sigma-Aldrich) and dissolved in the 99.9wt% of ethanol. The GDC powder and PVB dispersant take up 2 wt% of the ethanol respectively. Before mixing into the PVB dispersant, the precursor dissolved in the ethanol should go through the ball-milling process. Since the ball-milling process will make the powders dissolved more dispersive and reduce the agglomeration. The ball-milling process takes up about 24 h with the rotation rate of 150~160 r/min. After adding the PVB dispersant, we utilize the sonic device to get the precursor more dispersive.

The GDC layers were deposited on the commercial cells with a pre-determined optimum process condition such as solution flow rate 0.2 ml/h, nozzle-substrate distance 5.5 cm, deposition time 1 h, applied DC voltage 7.1kv.

After depositing 30min, then the samples were sintered in the furnace. The

sintering process like below:

(1) Post-annealed the sample to 200℃ at a heating rate of 2℃/min.

(2) Maintained at 200℃ for 2h.

(3) Annealed to 400℃ at the same heating rate.

(4) Maintained at 400℃ for 2h.

(5) Annealed to 1250℃ at the heating rate 2℃/min for 6 h.

(6) Maintained at 1250℃ for 2h.

(7) Gradually cooled the furnace to the room temperature in 5 h.

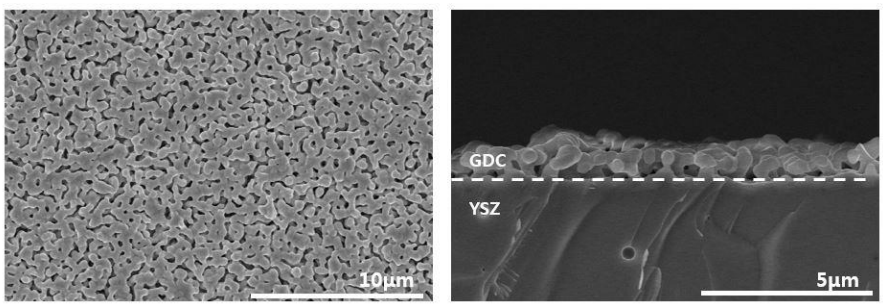

Figure 5 SEM images of the GDC layer

As shown in the figure 5, the GDC layer was about 300nm thick and pretty dense after sintering process. It uniformly covered the YSZ electrolyte and

adequately prevent the chemical reaction between the YSZ electrolyte layer and Cathode.

2.2. Cathode layer fabrication

As mentioned above, the cathode layer was composed of CFL and CCCL. CFL not only enhance the electrochemical performance of the cells, but also prevent the thermal mismatch during the annealing process.

The precursor solution of the CFL consisted of LSC(Kceracell) powder and GDC powder, whose mass ratio was 1:1, whose weight percent was 2.5wt% respectively. The solvent we applied was 94.5wt % ethanol. After ball- milling process, we added 5wt% PVP as the dispersant.

The CFL precursor solution was deposited on the GDC layer after annealing process. The flow rate was 0.2 ml/h, nozzle-substrate distance 4.5 cm, deposition time was 30 min and applied 5.8 kv DC voltage.

After depositing the CFL, we directly deposited CCCL before annealing process. The preparation process of the CCCL precursor solution was similar to the CFL. The solution was composed of 10wt% LSC and 10wt% PVP dispersant dissolved in 94.5wt% ethanol.

The ESD condition of the CCCL was the same as the CFL except the DC voltage was increased to 6.8 kv. And the deposition time also increased to 1h to insure the sufficient height of the cathode layer.

After all of the deposition process, we turn to annealing process. The

annealing steps of the cathode layer was like below:

(1) Post-annealed the sample to 200℃ at the heating rate 2℃/min.

(2) Maintained at the 200℃ for 2 h.

(3) Annealed to 400℃ at the same heating rate.

(4) Maintained at the 400℃ for 2 h.

(5) Annealed to 950℃ at a heating rate of 2℃/min for 5 h.

(6) Maintained at the 950℃ for 1 h.

(7) Gradually cooled the furnace to the room temperature in 4 h.

The integrated cells which were composed of anode, electrolyte, buffer layer, CFL and CCCL were shown in figure 6.

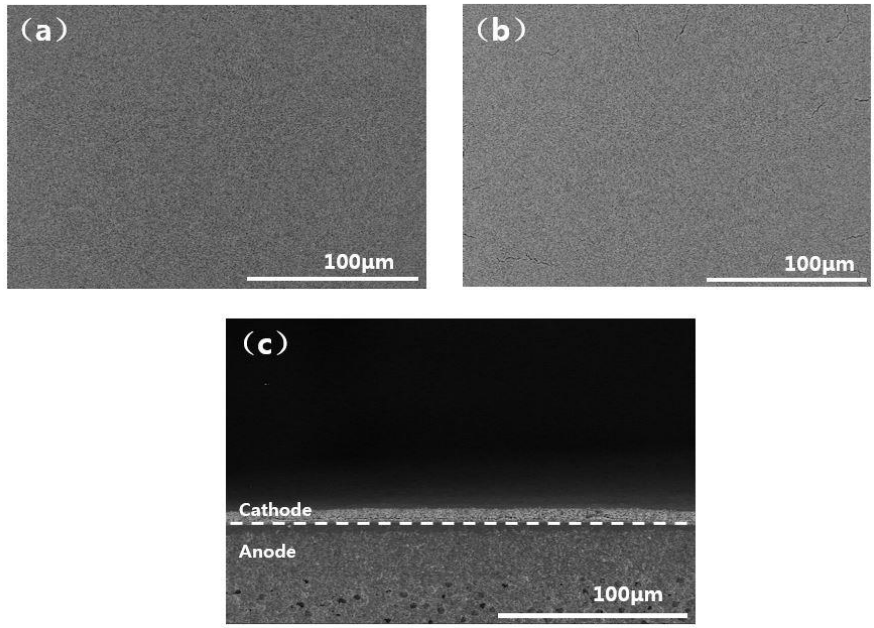

Figure 6 SEM images of (a)CFL (b)CCCL (c)integrated cell

From the figure 6, we could estimate that after the deposition and annealing process, the CFL and CCCL were uniformly deposited on the GDC layer. And the cathode layer was thick enough to take place the electrochemical reaction. The total thickness of the cathode is around 6μm.

Chapter 3. Crack-free cells' fabrication process

After fabricating the cells followed the steps mentioned above, we found there were many cracks on the surface of the cathode layer. From the research of the other experiments, the cracks occurred in the cathode layer are mainly on account of the thermal stress. And these cracks in the cathode may reduce the reaction area so that influence the ultimate performance of the cells.

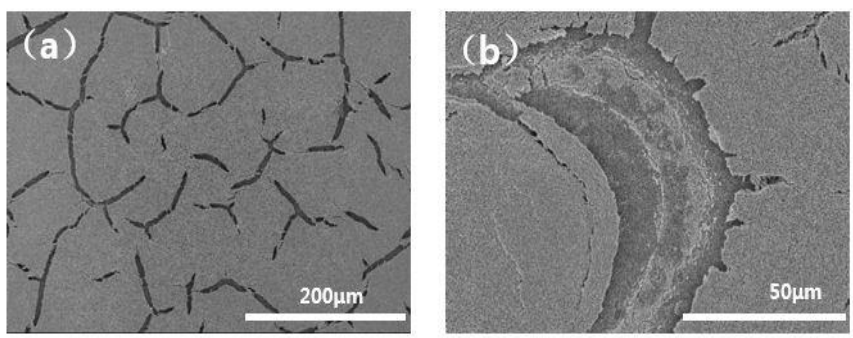

Figure 7 SEM images of cracks formation in the cathode layer

However, in the PA-ESD process to fabricate the SOFCs, the polymer dispersants are the main materials which are much more sensitive to the temperature than ceramic powders, which may cause a major thermal stress in the cathode layers.

Therefore, in order to decrease or remove the cracks in the cathode layer, we put forward three assumptions may influence the crack's formation in the PA-ESD process.

(1) The polymer species.

(2) The amount of polymer applied as dispersant.

(3) The deposition temperature via ESD process.

But what we can learn from the previous experiments, the polymer we can apply mostly in SOFCs' PA-ESD experiments, PVP and PVB are available. However, the PVB content in the precursor solution can't be too high. Because if the PVB content is too high, when the voltage is applied, the PVB will form the fiber and block the nozzle. So, PVB is not suitable for our experiments.

3.1. Adjusting the PVP polymer content

In order to analyze the connection between the polymer amount and cathode cracks formation. We displayed 4 groups of experiments. The amounts of PVP polymer in CCCL respectively were 2wt%, 5wt%, 10wt%, 20wt%, accordingly, the amount in CFL were 1wt%, 2.5wt%, 5wt%, 10wt%. The ratio of the PVP content and ceramic powder content was 1:1. So, in the CFL, the ratio of the GDC powder was 0.5wt%, 1.25wt%, 2.5wt%, 5wt%. And in the CCCL, the ratio tend to be 1wt%, 2.5wt%, 5wt%, 10wt%.

The process of the ESD deposition and annealing was same to the steps mentioned above, the only difference was when the powder content changed, we should adjust the applied voltage to avoid the formation of droplets.

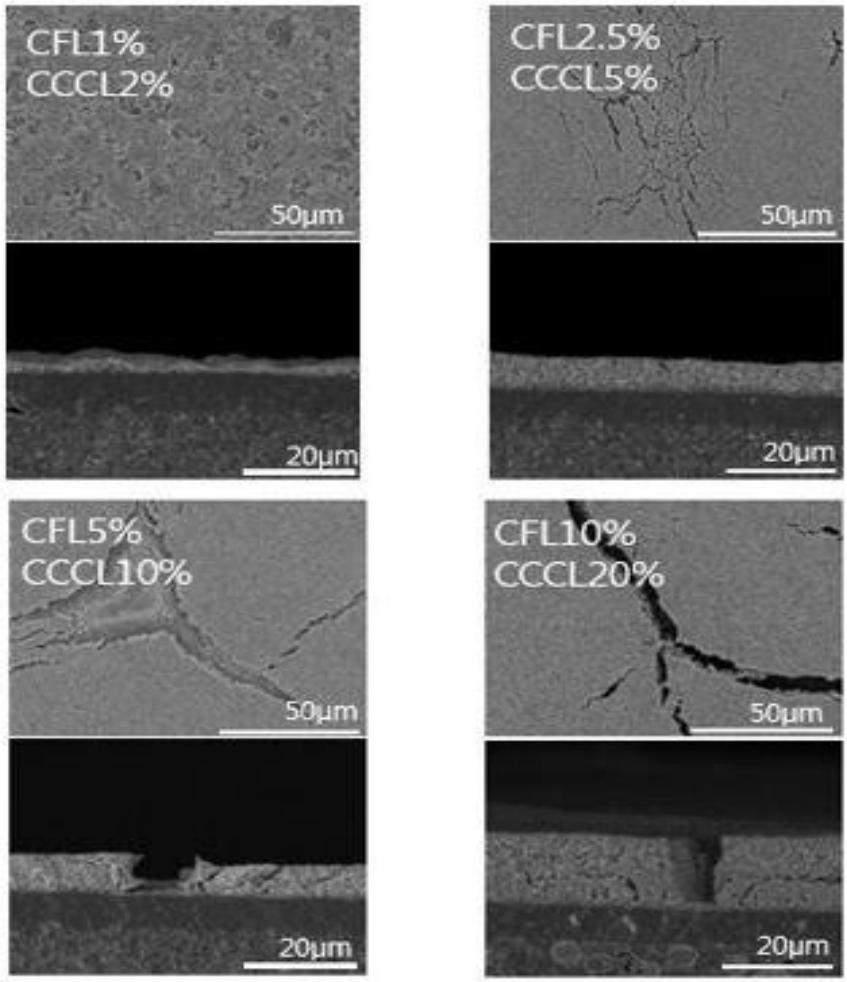

Figure 8 SEM images of the different PVP content cells

The figure 8 showed the SEM intuitionistic results of each experiment. We can estimate from the SEM images that the polymer amount may influence the morphology and structure of the cathode, but can't remove the formation of the cracks at all. Even though the cracks formation may be controlled when the weight percentage of polymer and ceramic powders are low, the cracks still

happened. And the smaller the content of the ceramic powders, the longer the deposition time. So, changing the PVP polymer amount to remover cracks seemed to be infeasible.

3.2. Adjusting the deposition temperature

At first, the reason why we put forward this assumption was that the PVP is one of the polymer and as we know, nearly all kinds of polymer are very sensitive to the temperature. Including the change of shape, viscosity and structure. The temperature plays a very important role to the PVP-assisted ESD process.

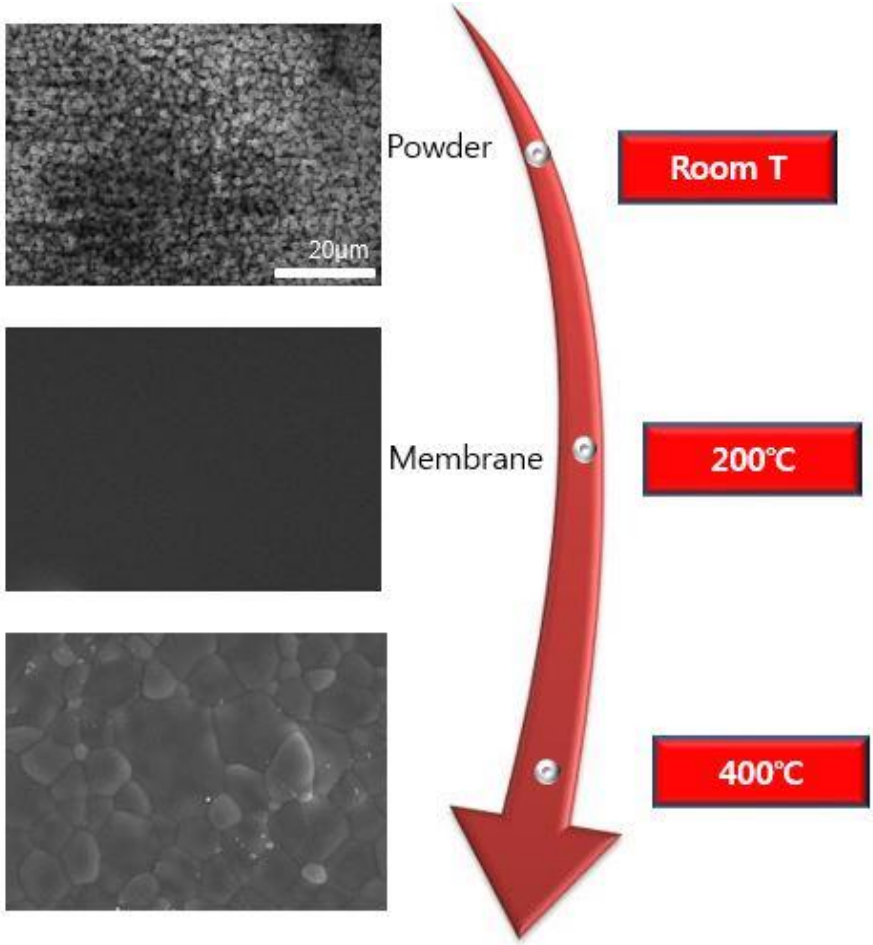

Figure 9 Only PVP deposited on the YSZ electrolyte and annealed to room temperature, 200℃ and 400℃

Figure 9 showed the SEM results of the morphology variation trend when sintered the only PVP deposited cells. When only PVP was deposited on the YSZ electrolyte, it presented the ball-shaped structure and deposited unevenly. But when the temperature is up to the 200℃, the polymer became a uniform membrane. When up to 400℃, PVP polymer was evaporated and there were

just bare YSZ left. From this, we can speculate that these kinds of initial morphologies' difference might have great influence to the ultimate cathode's final structure and morphology. Therefore, in order to explore the connection between the deposition temperature and the formation of cracks in the cathode, we displayed the following experiment.

As the intrinsic character of the polymer revealed, the polymer shape and modulus(E) change a lot when the temperature is ascending, especially near the glass transition temperature(Tg), this kind of change is tremendous So, we assumed that the Tg is the significant parameter during the experiment. Therefore, we utilized differential scanning calorimeter(DSC) to measure the PVP polymer's Tg.

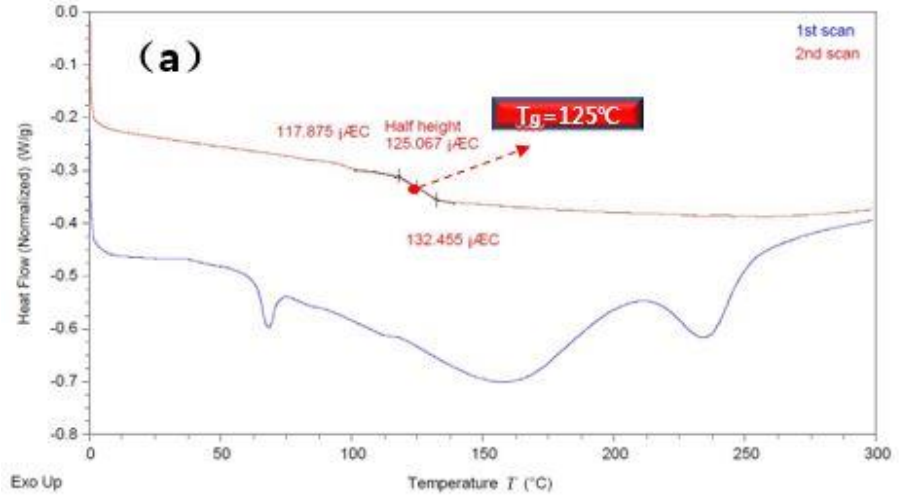

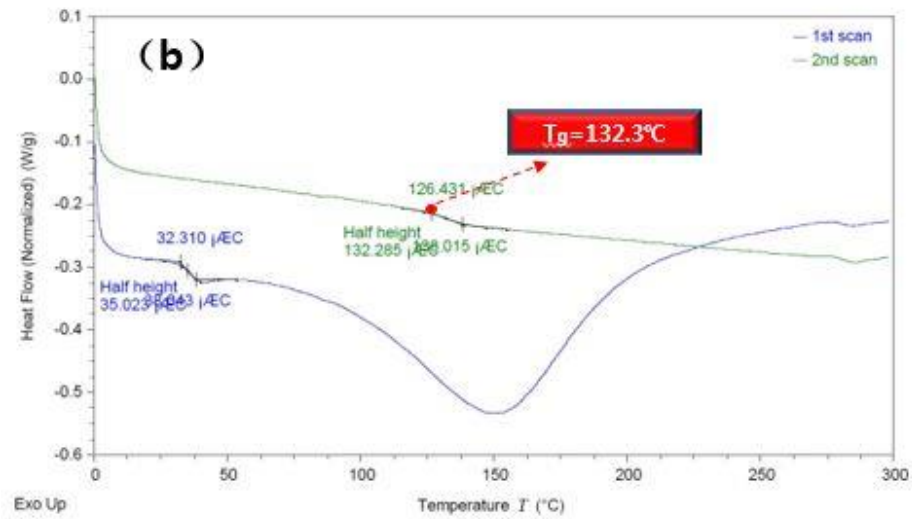

Figure 10 The DSC result of the (a) only PVP and (b) PVP+LSC

Figure10(a) showed the DSC result of the PVP, which revealed the glass transition temperature(Tg) of PVP was about 125℃. To figure out the influence of the LSC powder to the Tg of the PVP, we added the same mass of LSC powder

to the PVP polymer and tested DSC again. The figure6(b) showed the result of the Tg of the LSC and PVP mixture. From the comparison, we can conclude that the LSC may influence the Tg of the powder, but not distinct.

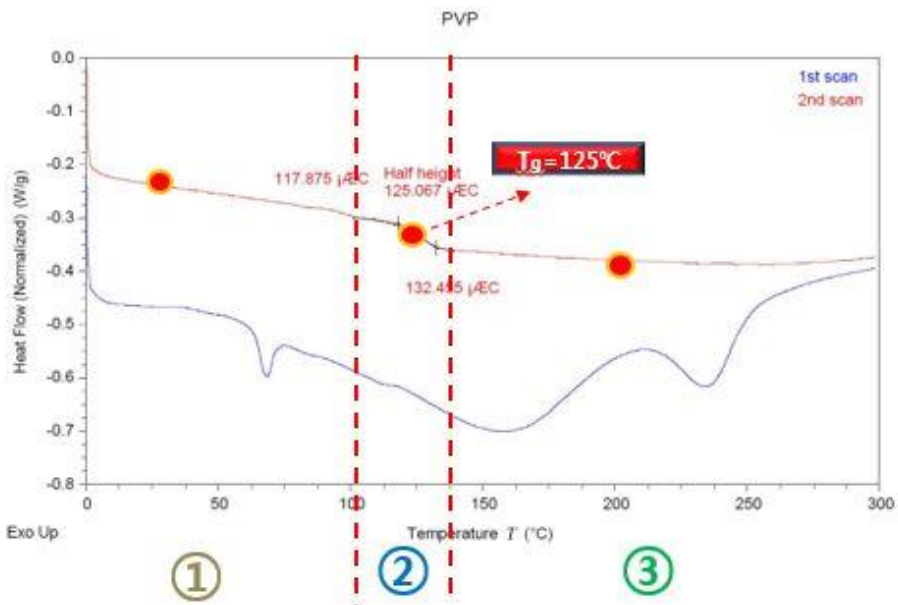

Figure 11 Schematic illustrations about the three temperature regions

Since the Tg of the PVP is around 125℃, we chose the three different temperature regions to verify our assumptions. The first region whose temperature was lower than Tg, we chose room temperature as the deposition temperature. In the second region, we chose 120℃ as deposition temperature, which is inter-glass transition temperature region and last one, we chose 200℃, which is much higher than Tg.

After depositing the CFL and CCCL, we sintered the samples followed the steps mentioned above. At this point, we should be careful that the cathodes' thickness will change if we adjust the deposition temperature. So, we accordingly adjust the deposition time to get the similar cathode thickness so as to compare the final performance. The SEM results of the samples were showed in figure 12

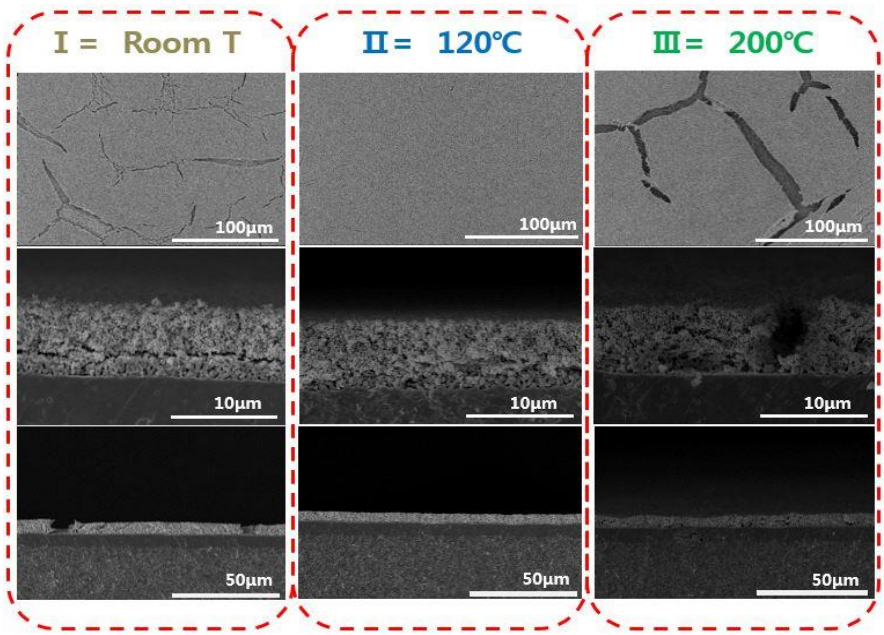

Figure 12 SEM images of cathodes deposited at room T, 120℃ and 200℃

Judged from the figure 12, it was obvious that the sample deposited at the 120℃ had much more uniform and crack-free structure and morphology. The samples deposited at room temperature and 200℃ were full of cracks. For the

further certification, we had tested the samples deposited with 80℃ and 160℃, too. The result was showed in figure 13.

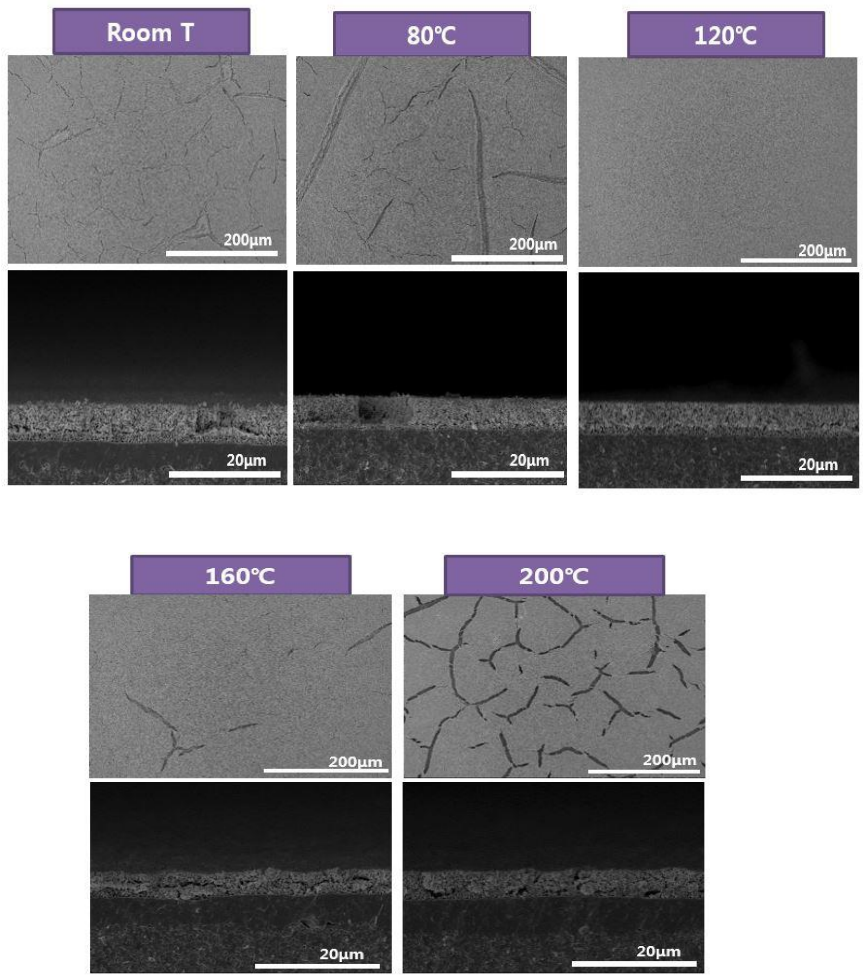

Figure 13 SEM images of cells deposited at room T, 80℃， 120℃， 160℃ and 200℃

From the figure 13, we can estimate that the cells deposited at the 80℃ and 160℃ conformed to the trend we have thought above. And clearly, the sample

with 120℃ deposition temperature was best both in structure and morphology.

The result of this group of experiments showed us that when the deposition temperature was around 120℃, the PVP assisted cathode will form the uniform and crack-free structure and morphology, and the 120℃ is in the vicinity of the PVP's glass transition temperature 125℃.

Chapter 4. The results of the cells' test

We have obtained two kinds of cells above, one is the cells full of cracks in the cathodes, the other is the crack-free cells deposited at 120℃. In order to compare the total cells' performance and check the influence of the cracks formation to the cells, we tested the cells with the three different deposition temperature-room temperature, 120℃and 200℃(Figure 14). It should be noted again that the cells used to deposit the GDC and cathode layers are all the same commercial cells from Nara-cell tech to minimize the other components' uncertainties in the experiment. Table 1 showed the testing result of the three cells. To clarify the dependence of the samples' electrochemical performance, I-V characteristics, and EIS results of the three different cells, we obtained the figures like below.

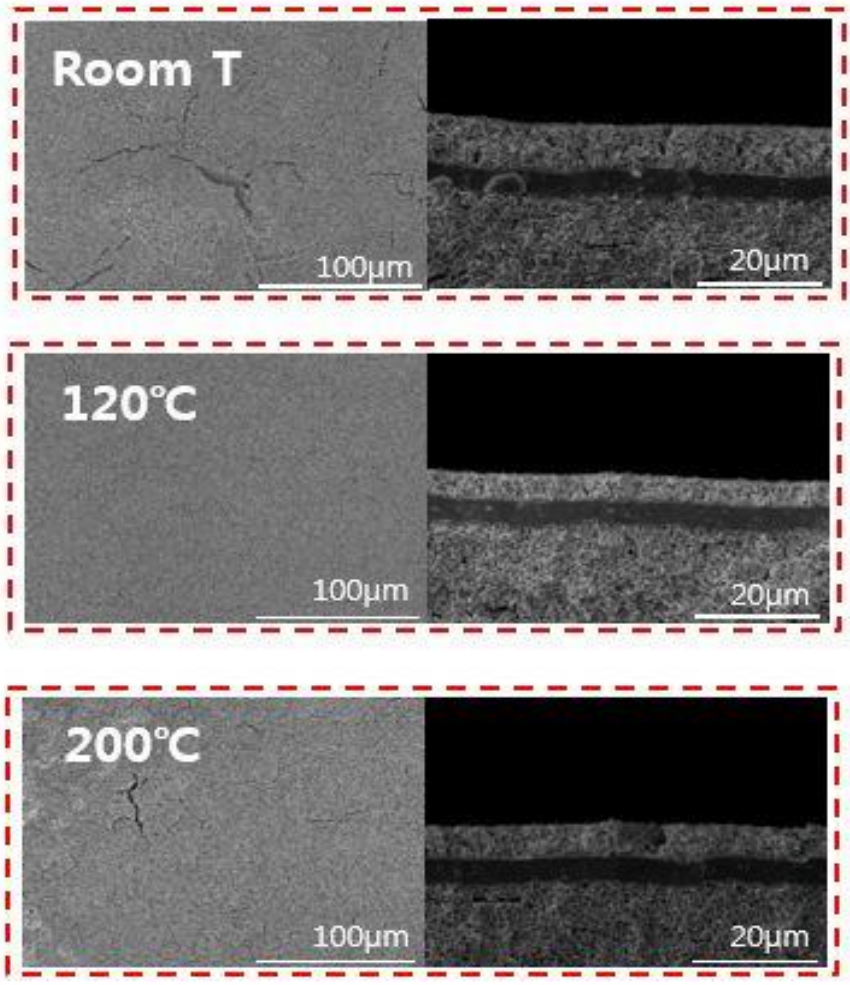

Figure 14 SEM images of tested cells

Table 1 Numerical value of the cells' test result

	Condition (Temp., Time)	OCV (V)	Ohm. ASR at OCV (Ω-cm²)	Pol. ASR at OCV (Ω-cm²)	Power Density at 0.7V (mW/cm²)	Peak Power Density (mW/cm2)
Room Temperature Cathode	650 ℃	1.093	0.294	1.51	269.115	349.6
	600 ℃	1.098	0.550	2.676	136.11	176.71
	550 ℃	1.109	1.001	7.264	51.825	64.26
	500 ℃	1.113	2.133	21.38	17.975	23.65
	Condition (Temp., Time)	OCV (V)	Ohm. ASR at OCV (Ω-cm²)	Pol. ASR at OCV (Ω-cm²)	Power Density at 0.7V (mW/cm²)	Peak Power Density (mW/cm2)
120℃ cathode	650 ℃	1.129	0.280	1.95	346.005	445.585
	600 ℃	1.136	0.447	3.131	185.5	237.075
	550 ℃	1.14	0.916	6.383	84.48	108.29
	500 ℃	1.182	1.653	18.277	25.165	35.105
	Condition (Temp., Time)	OCV (V)	Ohm. ASR at OCV (Ω-cm²)	Pol. ASR at OCV (Ω-cm²)	Power Density at 0.7V (mW/cm²)	Peak Power Density (mW/cm2)
200℃ cathode	650 ℃	1.121	0.290	2.886	240.81	346
	600 ℃	1.125	0.557	5.42	118.32	159.005
	550 ℃	1.13	1.24	15.25	41.82	54.5
	500 ℃	1.13	2.219	43.58	16.525	20.115

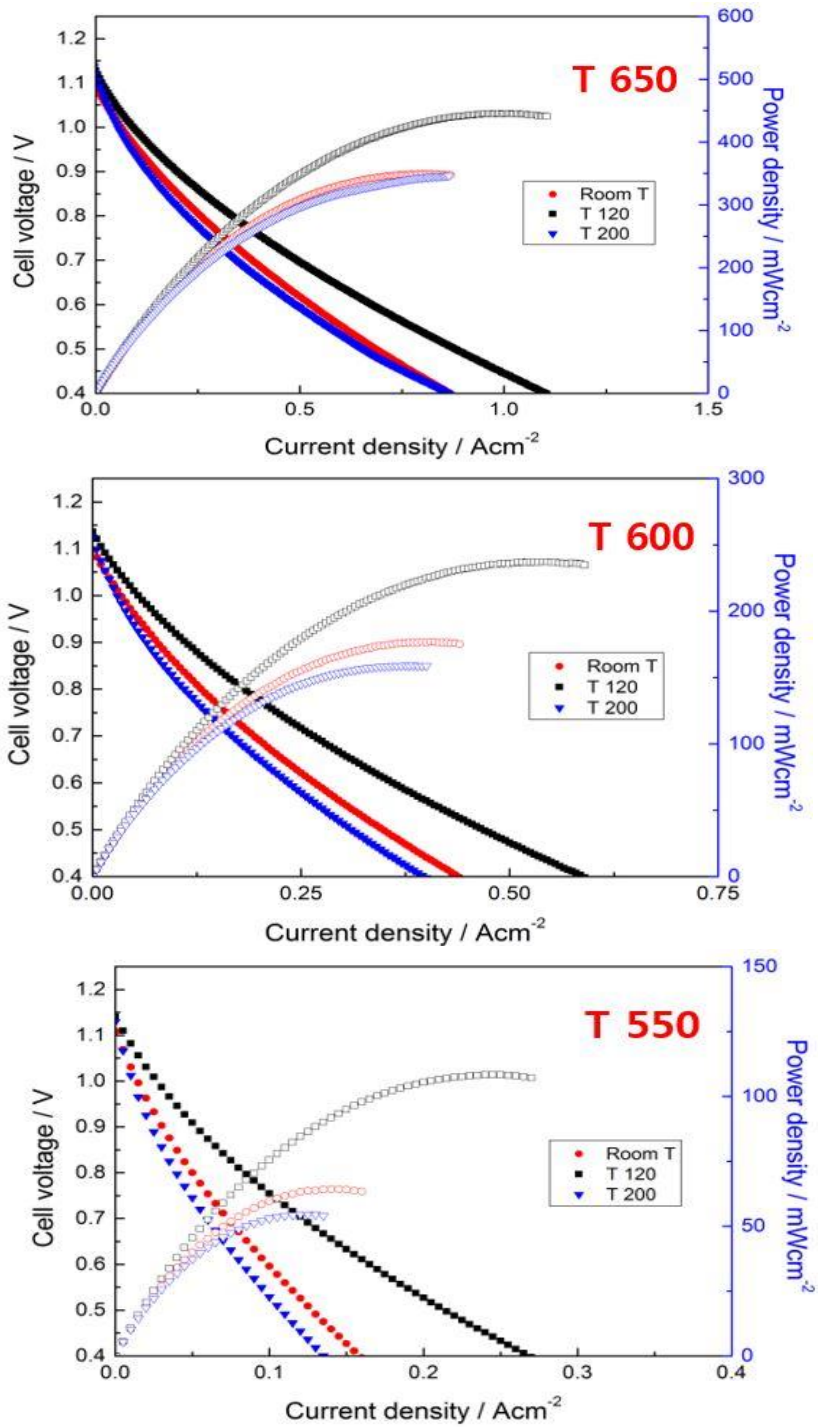

Figure 15 Electrochemical characterization of tested cells(I-V curves)

From the figure 15, all the measured OCV value of ~1.1V approached the theoretical value, indicating that the SOFCs we made were credible. And the maximum power density at 650℃ are 350mW/cm^2, 446mW/cm^2 and 347mW/cm^2 with the deposition temperature at room temperature, 120℃and 200℃ respectively. Also, when testing temperature are 600℃ and 550℃, the maximum power density also emerged at 120℃ deposition temperature. And from the figure, we can estimate that the lower the testing temperature, the better the crack-free cathode performed, too. The P_{max} at the deposition temperature 120℃ increased over 27.4% and 28.5% than deposited at room temperature and 200℃.

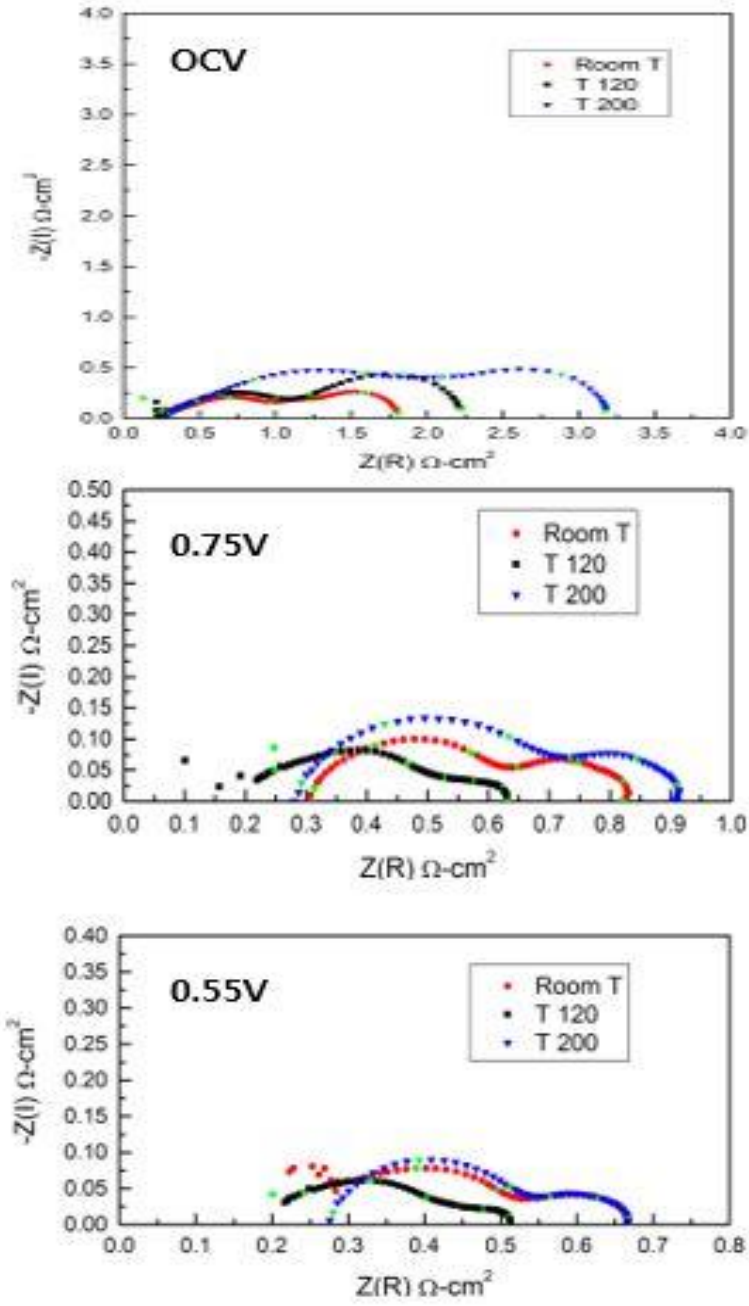

Figure 16 Electrochemical characterization of tested cells(EIS results)

AC impedance spectroscopy was carried out to further reveal which cell performs better. The results obtained during the testing temperature was 650℃, at the working voltage-OCV, 0.75V and 0.55V. From the figure,we can conclude that the cell which was deposited at 120℃ had better ohmic loss and polarization loss than the other two samples.

Chapter 5. Analysis

To figure out the reason why the cracks formation changes a lot with the deposition temperature, we have discovered the phenomenon with two different ways. One of them is using SEM images of different temperature annealed cells, to find the morphology and structure changing trend and intuitively observe the transformation. The other way is that making use of the stress measurement, to find out the internal stress variation trend in the cathode layer with different annealed temperature, and objectively depict the connection between the internal stress changing trend and the deposition temperature in the form of the rough graph. By using this graph, we can also nervily put forward some assumptions to account for the crack formation reasons

5.1 Analysis from SEM images

To intuitively observe the variation trend in structure and morphology of cathodes with different deposition temperature, we have prepared the samples deposited at room temperature, 120℃ and 200℃, then annealed these samples to the raw condition, 200℃, 400℃ and 950℃. From the figure 17, we can easily estimate that with the different deposition temperature, the initial morphologies and structures have great difference with each other. And these

kind of difference influence the ultimate conditions of the cathodes in spite of annealing to the same last temperature-950℃.

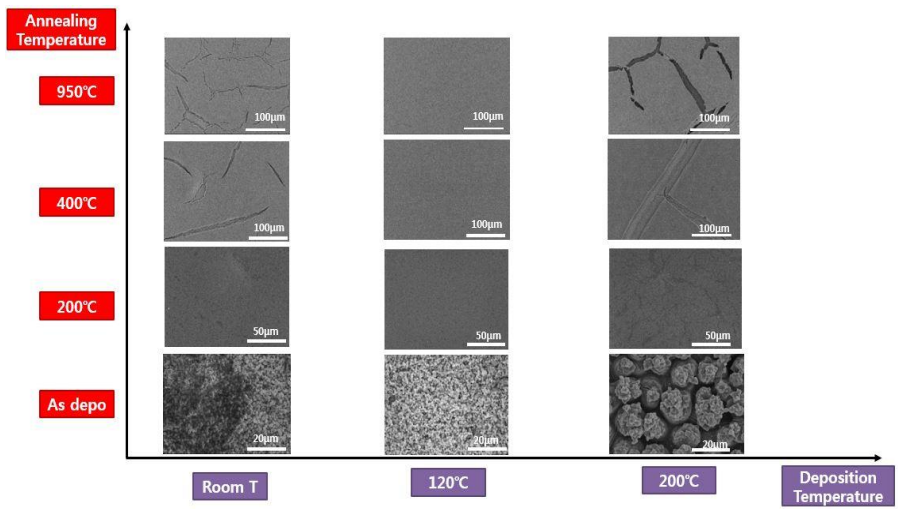

Figure 17 SEM images of cells with different treatments

We think that when deposited at the room temperature, the polymer PVP has no physical and chemistry variation, so the polymer and ceramic granule mixture has just emitted on the GDC layer and no displacement happened. On the contrary, when deposited at 120℃, the polymer-PVP's chain structure became flexible, and such freedom made the ceramic granule became more dispersive and removable. When we deposited at 200℃, the high temperature increased the PVP's fluidity, and in case of the hot plate temperature, the

velocity of the PVP's evaporation increased and these conditions enhanced the surface tension effect, resulting in the granules assemble together, forming the columnar-shaped structure.

To improve the importance of the initial deposition temperature further, we compared the following cases(figure 18). Although we annealed the samples to the same temperature we had deposited, the structures and morphologies had bid difference to each other.

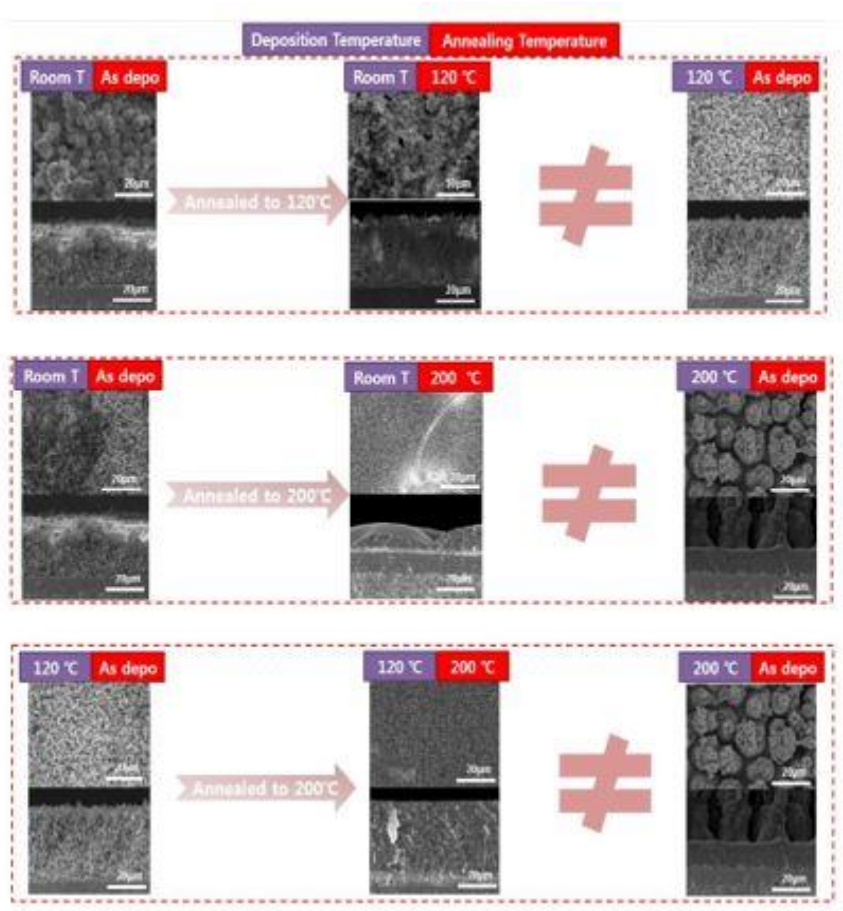

Figure 18 SEM images of cells with different treatments

Therefore, we can conclude that the variation of morphologies and structures in cathode layers caused by initial deposition temperature is very important and these kind of variation is irreversible.

5.2 Stress measurement analysis

To clarify the internal stress variation trend more objectively, we had measured the internal stress variation by 128&900 laser scanner. The principle of this device is that deposit the measured materials on the 4-inch wafer and annealed to the different temperature, because the wafer has nearly no flexibility, when the temperature was ascending, the materials deposited became shrunken and the wafer began to bend. With different annealing temperature, the degree of the bend was different. So, we can obtain the different curvature of the wafer by this device and substitute into the Stoney's Equation, we can easily get the cathode's stress variation trend.

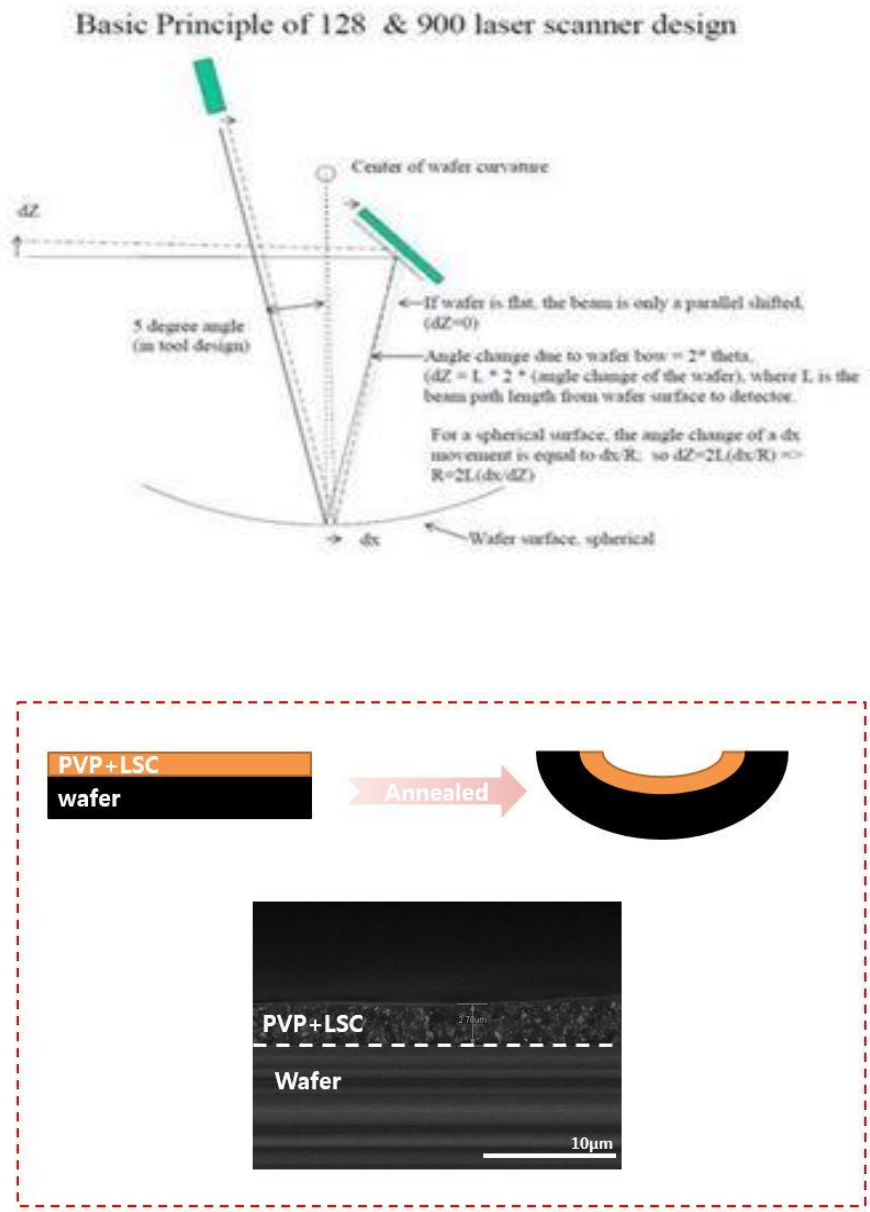

Figure 19 Principles of stress measurement

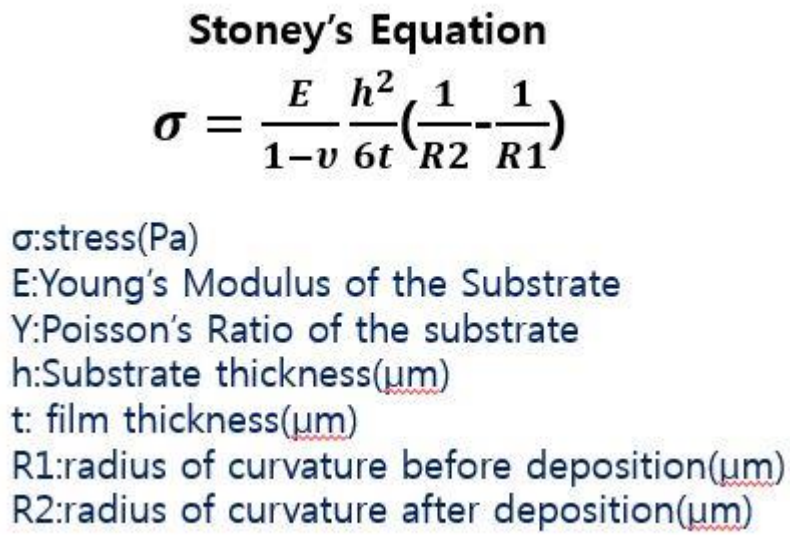

Figure 20 Stoney's Equation

However, this kind of measurement has two big uncertainties. One is that we deposited the cathode materials on the wafer instead of the commercial fuel cell we had utilized above. The difference in the wafer and ceramic materials must influence the result. But both of the wafer and sintered commercial cell have nearly no bendability, so we think the influence maybe not so much. The second uncertainty is that we deposit only the CCCL materials on the wafer in spite of the real cell has composite cathode, the exist of the CFL could reduce the thermal stress between the electrolyte and CCCL, so what we measured can't be correct. However, we think the magnitude of the curvature may change, but the variation trend of the it is consistent in both cases.

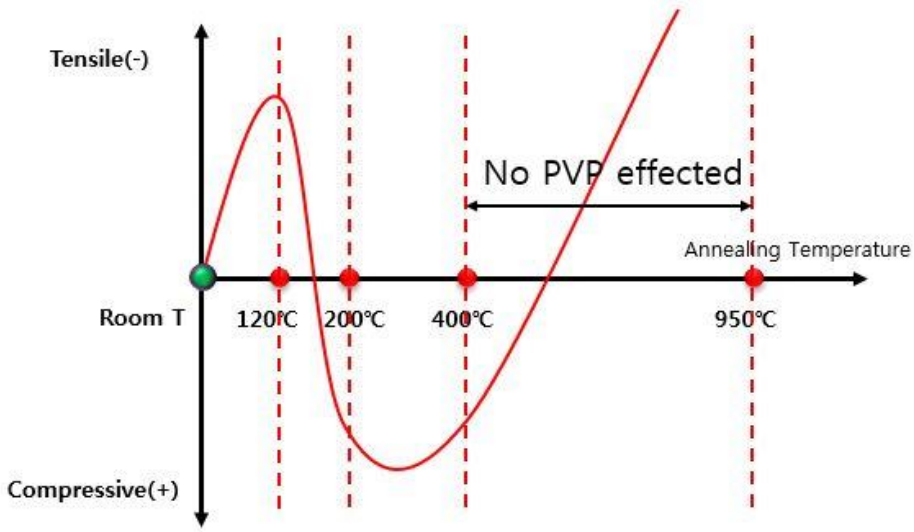

Figure 21 Rough graph depicted the internal stress's variation trend in the cathode layer

Under these premises, we drew the graphs to depict the internal stress variation trend. From the graph, when we assumed that the stress in the cathode layer at the room temperature is zero, the stress at 120℃ reached for the high point of tensile force. And with the temperature ascending, the tensile force began to decrease and at 200℃ the force became to be compressive. These kind of changes of force in the cathode layer must influence the cracks formation and propagation, and really helpful to find the right deposition temperature to make the cracks-free cells.

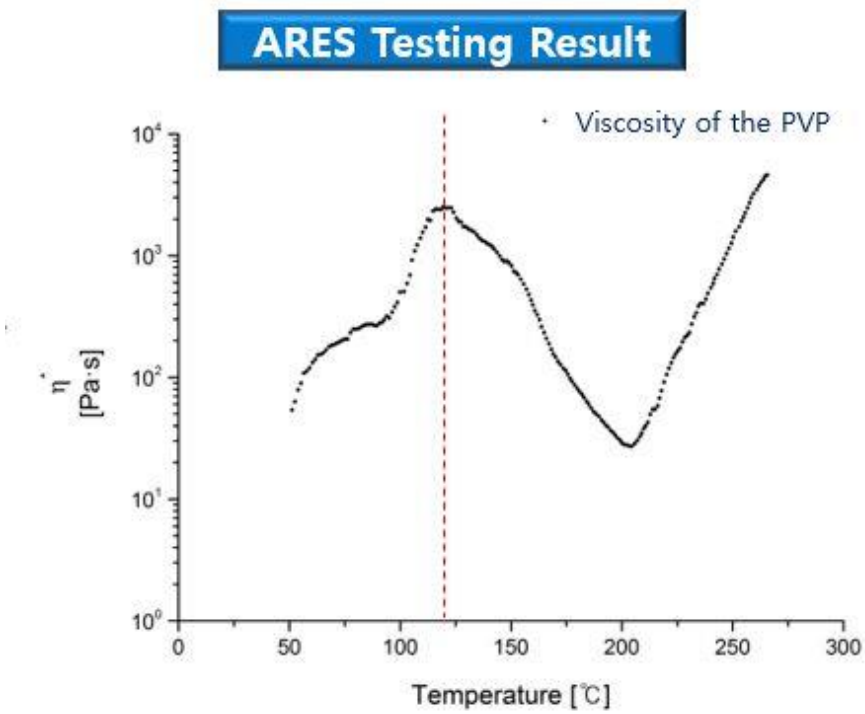

Figure 22 The ARES's result of PVP's viscosity variation trend with temperature

Before the measurement of the internal stress variation, in order to find out the character of the PVP polymer, we utilized the ARES(Advanced Rhemetric Expansion System) to measure the PVP's viscosity variation with the temperature. When we got the result from the stress measurement, we found the viscosity variation trend was almost consistent with the stress changing, and so, we boldly assumed that in PVP assisted ESD process to fabricate the SOFCs, the cracks formation and propagation have something to do with the PVP's viscosity.

Chapter 6. Conclusion

In summary, in this paper, we fabricated the pretty dense GDC barrier layer and porous CFL and CCCL on the commercial cells via ESD process. Using the way to adjust the deposition temperature, we effectively solved the cracks formation and propagation in the cathode layers. We built a novel parameter influencing the fabrication process of a dense thin electrolyte and a crack-free porous cathode as membrane components of a SOFC. We confirmed that the deposition temperature in the polymer-assisted ESD process was profound. Not only changing the structure and surface morphology of the cathode layer, but influencing the total performance of a SOFC. The SOFCs' performance applied PVP with deposition temperature 120℃ increased more than 25% than at room temperature and 200℃. And both ohmic and polarization loss reduced in the crack-free cathode SOFCs.

In addition, we found the internal stress in the cathode during annealing process is almost in accord with PVP's viscosity variation trend, so boldly assumed that paying attention to the polymer's viscosity variation trend was one of the way to distinctly improve a SOFC's performance via PA-ESD process by fabricating the crack-free cathode layers.

Bibliography

1. SUZUKI, Toshio, et al. Fabrication and characterization of micro tubular SOFCs for operation in the intermediate temperature. *Journal of Power Sources*, 2006, 160.1: 73-77.
2. Song, H. S., Hyun, S. H., Moon, J., & Song, R. H. (2005). Electrochemical and microstructural characterization of polymeric resin-derived multilayered composite cathode for SOFC. *Journal of power sources*, *145*(2), 272-277.
3. Fischer, W., Malzbender, J., Blass, G., & Steinbrech, R. W. (2005). Residual stresses in planar solid oxide fuel cells. *Journal of Power Sources*, *150*, 73-77.
4. Nguyen, B. N., Koeppel, B. J., Ahzi, S., Khaleel, M. A., & Singh, P. (2006). Crack growth in solid oxide fuel cell materials: from discrete to continuum damage modeling. *Journal of the American Ceramic Society*, *89*(4), 1358-1368.
5. Du, Y., & Sammes, N. M. (2004). Fabrication and properties of anode-supported tubular solid oxide fuel cells. *Journal of Power Sources*, *136*(1), 66-71.
6. Phair, J. W. (2008). Rheological analysis of concentrated zirconia pastes with ethyl cellulose for screen printing SOFC electrolyte films. *Journal of the American Ceramic Society*, *91*(7), 2130-2137.
7. Waldbillig, D., & Kesler, O. (2009). The effect of solids and dispersant loadings on the suspension viscosities and deposition rates of suspension plasma sprayed YSZ coatings. *Surface and Coatings Technology*, *203*(15), 2098-2101.

8. Yan, X. H., Zhao, T. S., An, L., Zhao, G., & Zeng, L. (2015). A crack-free and super-hydrophobic cathode micro-porous layer for direct methanol fuel cells. *Applied Energy*, *138*, 331-336.

9. Mogensen, M., Lybye, D., Bonanos, N., Hendriksen, P. V., & Poulsen, F. W. (2004). Factors controlling the oxide ion conductivity of fluorite and perovskite structured oxides. *Solid State Ionics*, *174*(1), 279-286.

10. Cook, R. L., & Sammells, A. F. (1991). On the systematic selection of perovskite solid electrolytes for intermediate temperature fuel cells. *Solid State Ionics*, *45*(3-4), 311-321.

11. Sammells, A. F., Cook, R. L., White, J. H., Osborne, J. J., & MacDuff, R. C. (1992). Rational selection of advanced solid electrolytes for intermediate temperature fuel cells. *Solid State Ionics*, *52*(1-3), 111-123.

12. Suzuki, T., Suzuki, T., Yamaguchi, T., Sumi, H., Hamamoto, K., Fujishiro, Y., & Shin, W. (2015). Fabrication and characterization of YSZ thin films for SOFC application. *Journal of the Ceramic Society of Japan*, *123*(1436), 250-252.

13. Chen, Y., Lin, Y., Zhang, Y., Wang, S., Su, D., Yang, Z., ... & Chen, F. (2014). Low temperature solid oxide fuel cells with hierarchically porous cathode nano-network. *Nano Energy*, *8*, 25-33.

14. Oh, D., Gostovic, D., & Wachsman, E. D. (2012). Mechanism of La 0.6 Sr 0.4 Co 0.2 Fe 0.8 O 3 cathode degradation. *Journal of Materials Research*, *27*(15), 1992-1999.

15. Ormerod, R. M. (2003). Solid oxide fuel cells. *Chemical Society Reviews*, *32*(1), 17-28.

16. Im, J., Park, I., & Shin, D. (2011). Electrochemical properties of nanostructured lanthanum strontium manganite cathode fabricated by electrostatic spray deposition. *Solid State Ionics*, *192*(1), 448-452.

17. Marinha, D., Rossignol, C., & Djurado, E. (2009). Influence of electrospraying parameters on the microstructure of La 0.6 Sr 0.4 Co 0.2 F 0.8 O 3− δ films for SOFCs. *Journal of Solid State Chemistry*, *182*(7), 1742-1748.

18. Princivalle, A., Perednis, D., Neagu, R., & Djurado, E. (2005). Porosity control of LSM/YSZ cathode coating deposited by electrospraying. *Chemistry of materials*, *17*(5), 1220-1227.

19. Gao, Z., Miller, E. C., & Barnett, S. A. (2014). A High Power Density Intermediate-Temperature Solid Oxide Fuel Cell with Thin (La0. 9Sr0. 1) 0.98 (Ga0. 8Mg0. 2) O3-δ Electrolyte and Nano-Scale Anode. *Advanced Functional Materials*, *24*(36), 5703-5709.

20. Lee, K. T., Lidie, A. A., Yoon, H. S., & Wachsman, E. D. (2014). Rational Design of Lower-Temperature Solid Oxide Fuel Cell Cathodes via Nanotailoring of Co-Assembled Composite Structures. *Angewandte Chemie International Edition*, *53*(49), 13463-13467.

21. Bozza, F., Polini, R., & Traversa, E. (2009). High performance anode-supported intermediate temperature solid oxide fuel cells (IT-SOFCs) with La 0.8 Sr 0.2 Ga 0.8 Mg 0.2 O 3− δ electrolyte films prepared by electrophoretic deposition. *Electrochemistry Communications*, *11*(8), 1680-1683.

22. Steele, B. C. H. (2001). Material science and engineering: the

enabling technology for the commercialisation of fuel cell systems. *Journal of Materials Science*, *36*(5), 1053-1068.

23. Wachsman, E. D., & Lee, K. T. (2011). Lowering the temperature of solid oxide fuel cells. *Science*, *334*(6058), 935-939.

24. Chen, Y., Zhou, W., Ding, D., Liu, M., Ciucci, F., Tade, M., & Shao, Z. (2015). Advances in cathode materials for solid oxide fuel cells: complex oxides without alkaline earth metal elements. *Advanced Energy Materials*, *5*(18).

25. Wang, S., Kato, T., Nagata, S., Honda, T., Kaneko, T., Iwashita, N., & Dokiya, M. (2002). Performance of a La 0.6 Sr 0.4 Co 0.8 Fe 0.2 O 3–Ce 0.8 Gd 0.2 O 1.9–Ag cathode for ceria electrolyte SOFCs. *Solid State Ionics*, *146*(3), 203-210.

26. Zhang, J., Ji, Y., Gao, H., He, T., & Liu, J. (2005). Composite cathode La 0.6 Sr 0.4 Co 0.2 Fe 0.8 O 3–Sm 0.1 Ce 0.9 O 1.95–Ag for intermediate-temperature solid oxide fuel cells. *Journal of Alloys and Compounds*, *395*(1), 322-325.

27. Haanappel, V. A. C., Rutenbeck, D., Mai, A., Uhlenbruck, S., Sebold, D., Wesemeyer, H., ... & Tietz, F. (2004). The influence of noble-metal-containing cathodes on the electrochemical performance of anode-supported SOFCs. *Journal of Power Sources*, *130*(1), 119-128.

28. Choi, H., Kang, S., Jung, W., Jung, Y. H., Park, S. J., Kim, D. S., & Choi, M. (2015). Controlled electrostatic focusing of charged aerosol nanoparticles via an electrified mask. *Journal of Aerosol Science*, *88*, 90-97.

29. Chueh, W. C., Hao, Y., Jung, W., & Haile, S. M. (2012). High

electrochemical activity of the oxide phase in model ceria-Pt and ceria-Ni composite anodes. *Nature materials*, *11*(2), 155.

30. Yang, Z., Hardy, J. S., Walker, M. S., Xia, G., Simner, S. P., & Stevenson, J. W. (2004). Structure and conductivity of thermally grown scales on ferritic Fe-Cr-Mn steel for SOFC interconnect applications. *Journal of the Electrochemical Society*, *151*(11), A1825-A1831.

31. Li, B., Liu, S., Liu, X., Hao, G., Wang, H., & Su, W. (2013). Study on GDC-LSGM composite electrolytes for intermediate-temperature solid oxide fuel cells. *International Journal of Hydrogen Energy*, *38*(26), 11392-11397.

32. Im, J., Park, I., & Shin, D. (2011). Electrochemical properties of nanostructured lanthanum strontium manganite cathode fabricated by electrostatic spray deposition. *Solid State Ionics*, *192*(1), 448-452.

33. Marinha, D., Rossignol, C., & Djurado, E. (2009). Influence of electrospraying parameters on the microstructure of La 0.6 Sr 0.4 Co 0.2 F 0.8 O 3− δ films for SOFCs. *Journal of Solid State Chemistry*, *182*(7), 1742-1748.

요약 (국문초록)

전기분사 공정을 이용한 고체산화물 연료전지 제작에서 증착온도가 미치는 영향

리 광 민

서울대학교 기계항공공학부기계전공 대학원

세라믹은 낮은 원가와 긴 수명 때문에 현재 중간온도에서 작동하는 고체산화물연료전지 생산에 적용되는 아주 유용한 재료로 손꼽히고 있다. 전기분사공정으로 고체산화물연료전지를 제작할 때 우리는 얇고 치밀한 YSZ 전해질층과 GDC 완충층을 성공적으로 제작하였다. 이 논문에서 우리는 전기분사공정으로 GDC와 LSC 혼합물로 이루어진 CFL과 LSC로 이루어진 CCCL 을 PVP 분산제를 사용하여 제작하였으며 제작 중에 생성되는 크랙에 관하여 연구하게 되었다. 실험 중 양극 층에 생성되는 크랙이 전기분사공정시 증착온도에 영향을 받고 있다는 것을 알게 되였으며 SEM 분석과 ARES 장비의 결과를 이용하여 크랙이 생성되는

이유와 해결 방법을 찾았다. 이를 통해 성능이 더 증가한 크랙없는 양극 층을 갖는 고체산화물 연료전지 제작에 성공하였으며, 다른 분산제를 사용하였을 때 적용할수 있는 제작방법도 제시하였다.

주요어: 고체산화물연료전지, PVP, cracks, 전기분사공정, 증착온도

학 번 : 2015-22304